

**GENERATION OF HIGH FREQUENCY P AND S WAVE  
ENERGY BY ROCK FRACTURE DURING A BURIED  
EXPLOSION: ITS EFFECT ON P/S DISCRIMINANTS  
AT LOW MAGNITUDES**

**Charles G. Sammis**

**University of Southern California  
Department of Earth Sciences  
3651 Trousdale Parkway  
Los Angeles, CA 90089-0740**

**1 December 2004**

**Final Report**

**APPROVED FOR PUBLIC RELEASE; DISTRIBUTION UNLIMITED.**



**AIR FORCE RESEARCH LABORATORY  
Space Vehicles Directorate  
29 Randolph Rd  
AIR FORCE MATERIEL COMMAND  
Hanscom AFB, MA 01731-3010**

---

This technical report has been reviewed and is approved for publication.

  
ROBERT RAISTRICK  
Contract Manager

  
ROBERT BELAND  
Branch Chief

This document has been reviewed by the ESC Public Affairs Office and has been approved for release to the National Technical Information Service (NTIS).

Qualified requestors may obtain additional copies from the Defense Technical Information Center (DTIC). All others should apply to the NTIS.

If your address has changed, if you wish to be removed from the mailing list, or if the addressee is no longer employed by your organization, please notify AFRL/VSIM, 29 Randolph Rd., Hanscom AFB, MA 01731-3010. This will assist us in maintaining a current mailing list.

Do not return copies of this report unless contractual obligations or notices on a specific document require that it be returned.

# REPORT DOCUMENTATION PAGE

Form Approved  
OMB No. 0704-0188

Public reporting burden for this collection of information is estimated to average 1 hour per response, including the time for reviewing instructions, searching existing data sources, gathering and maintaining the data needed, and completing and reviewing this collection of information. Send comments regarding this burden estimate or any other aspect of this collection of information, including suggestions for reducing this burden to Department of Defense, Washington Headquarters Services, Directorate for Information Operations and Reports (0704-0188), 1215 Jefferson Davis Highway, Suite 1204, Arlington, VA 22202-4302. Respondents should be aware that notwithstanding any other provision of law, no person shall be subject to any penalty for failing to comply with a collection of information if it does not display a currently valid OMB control number. **PLEASE DO NOT RETURN YOUR FORM TO THE ABOVE ADDRESS.**

**1. REPORT DATE (DD-MM-YYYY)**

01-12-2004

**2. REPORT TYPE**

Final

**3. DATES COVERED (From - To)**

SEP 2001 to SEP 2004

**4. TITLE AND SUBTITLE**

Generation of High Frequency P and S Wave Energy by Rock Fracture  
During a Buried Explosion: Its Effect on P/S Discriminants at Low Magnitudes

**5a. CONTRACT NUMBER**

DTRA01-01-C-0086

**5b. GRANT NUMBER****5c. PROGRAM ELEMENT NUMBER****6. AUTHOR(S)**

Charles G. Sammis

**5d. PROJECT NUMBER**

DTRA

**5e. TASK NUMBER**

OT

**5f. WORK UNIT NUMBER**

A1

**7. PERFORMING ORGANIZATION NAME(S) AND ADDRESS(ES)**

University of Southern California  
Department of Earth Sciences  
3651 Trousdale Parkway  
Los Angeles, CA 90089-0740

**8. PERFORMING ORGANIZATION REPORT NUMBER****9. SPONSORING / MONITORING AGENCY NAME(S) AND ADDRESS(ES)**

Air Force Research Laboratory  
29 Randolph Road  
Hanscom AFB, MA 01731-3010

**10. SPONSOR/MONITOR'S ACRONYM(S)****11. SPONSOR/MONITOR'S REPORT NUMBER(S)**

AFRL-VS-HA-TR-2004-1208

Contract Manager: R. Raistrick AFRL/VSBYE

**12. DISTRIBUTION / AVAILABILITY STATEMENT**

Approved for Public Release; Distribution Unlimited.

**13. SUPPLEMENTARY NOTES****14. ABSTRACT**

High stresses in the source volume of an underground explosion produce a shell of crushed and fractured rock surrounding the shot point. We have modeled this process using a micro-mechanical damage mechanics in an effective medium source model to calculate the nucleation, growth, and interaction of fractures from an array of preexisting flaws. We have found that the nucleation and growth of fracture damage generates secondary seismic radiation that can be comparable in amplitude to the radiation generated by the pressure pulse itself. This secondary radiation is higher frequency than the primary radiation and can have a large shear wave component if there is a preferential orientation of the initial flaws or if there is a significant regional pre-stress field. It can be significant in the interpretation of regional discriminants that use local S phases. We have explored the scaling properties of this secondary radiation by modeling the chemical NPE explosion and US nuclear explosions in granite: HARDHAT, SHOAL, and PILEDRIVER. Finally, we have initiated work to understand the effect of frozen rock at the source point on the seismic coupling in hard rock. Existing data can be explained if ice controls the sliding friction on preexisting cracks.

**15. SUBJECT TERMS**

Underground explosion, Seismic source, Damage mechanics, Non-linear rheology, Seismic coupling in frozen rock

**16. SECURITY CLASSIFICATION OF:**

a. REPORT  
UNCLAS

b. ABSTRACT  
UNCLAS

c. THIS PAGE  
UNCLAS

**17. LIMITATION OF ABSTRACT**

SAR

**18. NUMBER OF PAGES****19a. NAME OF RESPONSIBLE PERSON**

Robert J. Raistrick

**19b. TELEPHONE NUMBER (include area code)**

781-377-3726

## ABSTRACT

High stresses in the source volume of an underground explosion produce a shell of crushed and fractured rock surrounding the shot point. We have modeled this process using a micro-mechanical damage mechanics, which calculates the nucleation, growth, and interaction of fractures from an array of preexisting flaws. In previous studies, we have shown that this fracture damage can have a significant effect on the waveform of the seismic radiation. In particular, it explains the pulse broadening and overshoot observed in the seismic pulse from large explosions in hard rock, but not simulated by models which do not include dynamic fracture damage in the source. In collaboration with other groups, we have incorporated our damage mechanics into numerical source codes and into a simpler effective medium source model.

We have also found that the nucleation and growth of fracture damage generates secondary seismic radiation that can be comparable in amplitude to the radiation generated by the pressure pulse itself. At the very end of the prior contract period, Lane Johnson and the PI used the equivalent medium source model to calculate the seismic radiation at a distant observation point from each small crack in the damage zone. Because our damage mechanics is micromechanical, we could calculate the dilatational and shear moment tensors for each crack. While the radiation from each crack is small and very high frequency, the integrated effect of the coherent triggering of a large volume of cracks by the explosive stress pulse produced a large signal in the seismic frequency band. This secondary radiation is higher frequency than the primary radiation and can have a large shear wave component if there is a preferential orientation of the initial flaws or if there is a significant regional pre-stress field. It can be very significant in the interpretation of regional discriminants that use local S phases. We validated our source model using near-field data from the NPE chemical explosion.

During the current contract period we have explored the scaling properties of this secondary radiation by modeling the US nuclear explosions in granite: HARDHAT, SHOAL, and PILEDRIIVER. Also, at the very end of the current contract period, we have initiated work to understand the effect of frozen rock at the source point on the seismic coupling of an underground explosion in hard rock. We have shown that the limited amount of current data on the strength of frozen rock as a function of temperature below the freezing point can be explained if ice controls the sliding friction on preexisting cracks. The net result is a smaller apparent source with less secondary radiation for a given yield.

Key words: underground explosion, seismic source, damage mechanics, non-linear rheology, seismic coupling in frozen rock

## INTRODUCTION

The overall objective of this research program has been to incorporate damage mechanics in the numerical codes used to simulate underground nuclear explosions. This work was originally motivated by discrepancies between theoretical and observed seismic waveforms produced by explosions in crystalline rock that were tentatively ascribed to the extensive fracturing and granulation of the rock in the non-linear source region. We quantified this process by incorporating the micromechanical model-based damage rheology developed by Ashby and Sammis (1990) into two quite different source models: the effective medium source model developed by Lane Johnson and the more traditional finite difference model used by Jeff Stevens and his collaborators. Results of these simulations are reported by Rimer et al. (1999) and Stevens et al., (2002).

As a part of the Johnson and Sammis (2001) study, we found that the damage process itself can generate significant high frequency P wave energy and also S wave energy if there is a preferred regional pre-stress direction, or if the initial damage has a preferential orientation, or both. This research is relevant to the program because recent advances in seismic discrimination and yield estimate of underground nuclear explosions have been based largely on high-frequency local phases such as  $L_g$  and higher-mode surface waves. This shift in focus to higher frequencies has stimulated new interest in understanding the non-linear seismic coupling near the source.

In this study, we have applied the Johnson and Sammis (2001) analysis to the US nuclear explosions in granite (HARDHAT, SHOAL, and PILEDIVER) in order to study the scaling of secondary P and S wave radiation with yield. We have also begun to analyze the effect of frozen rock on the seismic coupling. Our first step has been to use the Ashby and Sammis (1990) damage mechanics to explain the little bit of laboratory data that currently exists on the strength of rock as a function of temperature below zero degrees Celsius.

### Non-linear Regimes in the Source Region of An Underground Explosion

Several different processes occur in the rock near a tamped underground explosion as illustrated in Figure 1 (see, e.g., Rodean, 1971). The explosion is initially contained within a cavity of radius  $r_c$ , which has been excavated from the surrounding rock. At the time of detonation a hot pressurized gas is created within the cavity, which causes it to expand. Some of the surrounding rock may be vaporized and added to the cavity gas at this time. The sudden expansion of the cavity generates a shock wave that propagates outward causing major damage to the surrounding rock and producing the series of regimes summarized in Figure 1. Rock first flows plastically; then is stressed beyond its brittle failure limit and becomes granulated; then is stressed to the point where radial cracks grow but failure is not reached; then deforms anelastically where pre-existing cracks slide but do not grow; and finally deforms elastically. These regimes reflect the decrease in energy density in the shock with distance from the explosion caused partly by spherical spreading and partly by the fact that energy is being used to fracture and deform the rock. The shock wave gradually decays into an inelastic wave involving non-linear motions, which further decays with distance until a radius is reached where the motions are small enough to be described by the ordinary elastodynamic equations of linear elasticity. Beyond this elastic

radius,  $r_e$ , the disturbance caused by the explosion can be modeled as linear elastic waves that propagate throughout the rest of the earth.

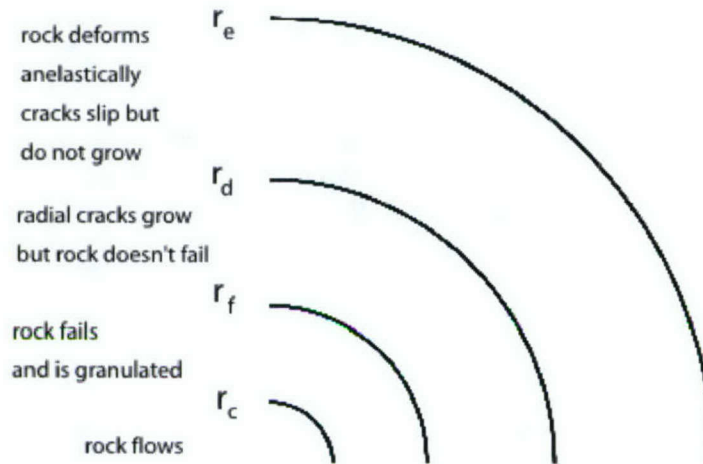


**Figure 1.** Schematic diagram of the region surrounding a contained explosion in rock:  $r_c$  is the cavity radius,  $r_f$  is the radius to which failure occurs,  $r_d$  is the radius to which new damage is created, and  $r_e$  is the elastic radius beyond which waves can be approximated as elastic.

These processes that occur around an explosion can have strong effects on the elastic waves that are radiated beyond the elastic radius  $r_e$ . In this report we concentrate on the growth of pre-existing cracks that can affect the radiated elastic waves in at least three different ways. First, intense cracking will significantly lower the bulk modulus and shear modulus near the source (O'Connell and Budianski, 1974; Rimer et al. 1998). Second, it has been speculated that when cracking extends into the failure regime, acoustic fluidization can lower the basic strength of the rock (Sammis, 1998). Third, motions on the cracks serve as secondary sources of elastic waves that can contribute to the net seismic radiation field. The primary objective of the work reported here is to provide a quantitative assessment of this third phenomenon. The intent is to determine how these secondary sources modify the P and S waves generated by the explosion and radiated to the far field.

We approach this problem by using the formulation of Ashby and Sammis (1990) to model the nucleation and growth of cracks in the source region, which is here referred to as damage. Calculation of this damage requires knowledge of the stress field in the region surrounding the source, which is approximated in this study by the equivalent elastic method. The micro-mechanical model of damage provides the parameters necessary to represent each crack as a seismic moment tensor that is then used to calculate the elastic waves radiated by the damage. Finally, we consider the cumulative effect of all the cracks in the damage zone in order to estimate the contribution of damage to P and S waves in the far field.

### Micromechanical Damage Mechanics

The concept of damage used here is that developed by Ashby and Sammis (1990). In that paper, the conditions under which an initial crack can nucleate additional cracking are derived. Only the basic equations needed to calculate the increase in damage at the shock front will be repeated here. In 3D the initial damage is defined as

$$D_0 = \frac{4}{3} \pi (a \cos \chi)^3 N_V, \quad (1)$$

where  $a$  is the radius of penny-shaped cracks,  $\chi$  is angle describing the orientation of the cracks (see Figure. 2) and  $N_V$  is the number of cracks per unit volume. In response to loading, wing cracks of length  $l$  grow at opposite edges of the initial crack thereby increasing the damage to

$$D = \frac{4}{3} \pi (l + a \cos \chi)^3 N_V. \quad (2)$$

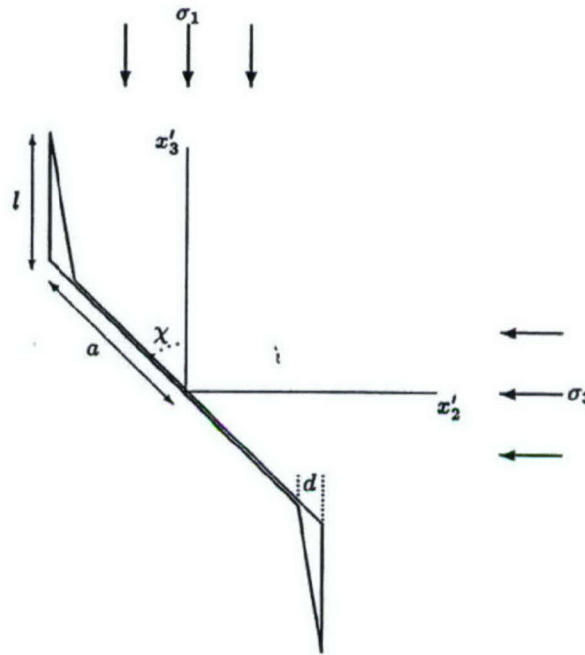


**Figure 2.** Geometry of a penny-shaped crack of radius  $a$ , which is extended by wing cracks of length  $l$ .

The value of  $l$  is determined by letting the wing cracks grow until the stress intensity factor at the tip decreases to the fracture toughness of the medium. The equation that must be solved to determine the final amount of damage is (Ashby and Sammis, 1990)

$$S_1 = - \frac{C_2 \left( \left( \frac{D}{D_0} \right)^{1/3} - 1 + \frac{\beta}{\cos \chi} \right)^{2/3} - S_3 \left[ C_1 \left( 1 + \left( \frac{C_3 D_0^{2/3}}{1 - D^{2/3}} \right) \left( \left( \frac{D}{D_0} \right)^{1/3} - 1 \right)^2 \right) + C_4 \left( \left( \frac{D}{D_0} \right)^{1/3} - 1 \right)^2 \right]}{1 + \frac{C_3 D_0^{2/3}}{1 - D^{2/3}} \left( \left( \frac{D}{D_0} \right)^{1/3} - 1 \right)^2} \quad (3)$$

Here  $S_1$  and  $S_3$  are the maximum and minimum normalized principal compressive stresses given by

$$S_1 = \frac{\sigma_1}{K_{Ic}/\sqrt{\pi a}}, \quad S_3 = \frac{\sigma_3}{K_{Ic}/\sqrt{\pi a}} \quad (4)$$

and  $K_{Ic}$  is the critical stress intensity for mode I cracks, a material property. The constants in (3) are

$$\begin{aligned} C_1 &= \frac{(1+\mu^2)^{1/2} + \mu}{(1+\mu^2)^{1/2} - \mu} \\ C_2 &= \pi(\cos \chi)^{3/2} \sqrt{3/\beta} \frac{1}{(1+\mu^2)^{1/2} - \mu} \\ C_3 &= 2 \\ C_4 &= 2\pi(\cos \chi)^2 \sqrt{3/\beta} \frac{1}{(1+\mu^2)^{1/2} - \mu} \end{aligned} \quad (5)$$

In these last equations,  $\mu$  is the coefficient of static friction and  $\chi$  is a correction factor for the effective length of the crack, typically 0.45 introduced by Ashby and Sammis (1990) to bring their approximate analytical model into agreement with numerical simulations in the limit of small  $l$ . Also,  $\chi$  is assumed here to be  $45^\circ$ .

Given the initial damage  $D_0$  and the principal stresses  $\sigma_1$  and  $\sigma_3$ , equation (3) can be used to calculate the equilibrium state of damage. This is a cubic equation in the damage, which we solve numerically. There are three possible outcomes. At low stresses, wing cracks do not nucleate and we get no real solutions. At intermediate stresses we calculate a value of  $D > D_0$  until a maximum is reached above which we again get no real solutions. Ashby and Sammis (1990) interpret this maximum as failure since, for additional loading, damage increases at decreasing stress, an unstable condition leading to shear localization. We do not attempt to model this post-failure regime beyond identifying it as the granulated region described in the introduction, and as a possible site for further weakening by acoustic fluidization. Figure below shows a conceptual model of how damage is generated in the stress field at the shock front of the explosion. In this case the principal stresses are the radial and hoop stress in the spherical geometry.

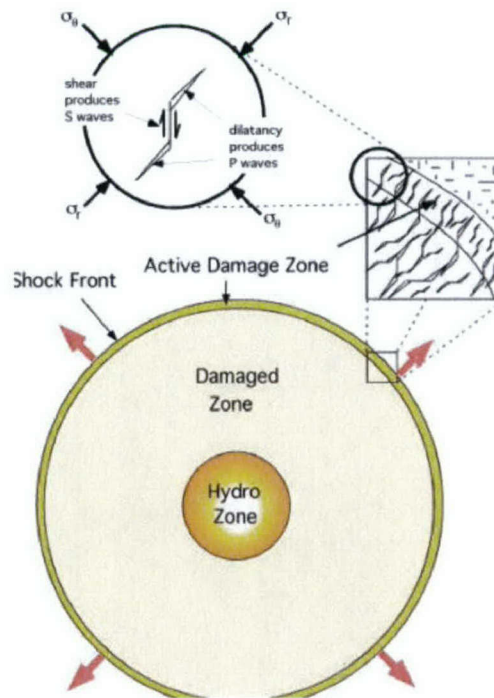


**Figure 3.** Generation of fracture damage in the shock front of an underground explosion.

#### *Stress Field Surrounding an Explosion – The Effective Elastic Medium*

In order to model the increase in damage we require the principal stresses generated by the explosion as a function of distance and time. This is made difficult by the existence of the nonlinear processes between the cavity radius and the effective elastic radius, beyond which the assumptions of ordinary linear elasticity are valid. Sophisticated computer codes have been developed which include hydrodynamic effects, shock waves, and nonlinear equations of state (see, for example, Rodean, 1971; King et al., 1989; Glenn, 1993; Glenn and Goldstein, 1994, for discussion and further references). We use here an approximate method to calculate the stresses surrounding an explosion that is based on the equivalent elastic method developed by earthquake engineers to model the nonlinear behavior of soils that occurs during strong ground motion. The central idea is to make the material properties a function of the stress in the outward propagating pressure pulse and then to adjust these material properties in an iterative process until the appropriate values are present at all distances from the source. In effect, the nonlinear stress-strain behavior is approximated by a series of linear relationships that change with the level of stress. The present formulation, described by Johnson (1993), relates density and bulk elastic properties to the peak pressure and shear and anelastic properties to the maximum shear strain.

The details of this model are published in Johnson and Sammis (2001) and will not be repeated here. In that paper we modeled the 1 kt chemical explosion detonated in September 1993 as part of the Non-Proliferation Experiment (NPE) (see Denny, 1994). The results of this simulation and attendant damage calculations are summarized in the next section where it is compared with new calculations for US explosions in granite: HARDHAT, SHOAL, and PILEDIVER.

### Secondary seismic radiation from damage

Since Ashby and Sammis (1990) model damage as a collection of initial cracks that are extended by wing cracks, each element of this damage may be represented as the combination of two separate source moment tensors: shear dislocation on the initial crack gives a scalar moment tensor per unit volume of

$$m_s = \frac{9}{2} \frac{\lambda + 2\mu}{\lambda + \mu} \frac{K_{Ic}}{(\pi a \cos \chi)^{1/2}} \frac{D_0}{\sin \chi \cos^2 \chi} \left[ \left( \frac{D}{D_0} \right)^{1/3} - 1 \right]^{1/2} \quad (6)$$

while tensile opening of the wing cracks gives

$$m_t = \frac{3(\lambda + 2\mu)^2}{2\mu(\lambda + \mu)} \frac{K_{Ic}}{(\pi a \cos \chi)^{1/2}} D_0 \left[ \left( \frac{D}{D_0} \right)^{1/3} - 1 \right]^{5/2} \quad (7)$$

A complete specification of the moment tensor for the damage requires that the orientation of the cracks be considered. We did this by transforming the local coordinates of the initial cracks (which varied with position around the source) to a fixed coordinate system for wave propagation to a specified field point. These transformations are straightforward but messy and are given in Johnson and Sammis (2001).

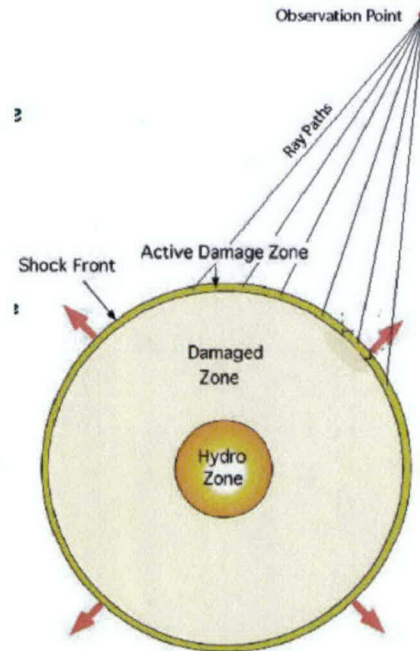


**Figure 4.** Integrating active damage to calculate secondary radiation at the observation point. Although each individual crack only contributes a small amount at high frequency, the integrated effect is to create seismic radiation comparable to that generated directly by the explosion.

Results for the NPE explosion

The results from Johnson and Sammis (2001) are summarized in the following two Tables.

**Table 1.** Effect of the initial damage on source parameters for starter flaw with  $a=0.1$  cm.  
See Figure 1 for definitions of the various radii.  
(from Johnson and Sammis, 2001)

| $D_0$ | $D_f$ | $r_f$<br>(m) | $r_d$<br>(m) | $V_{max}$<br>(cm/sec) |
|-------|-------|--------------|--------------|-----------------------|
| 0.01  | 0.09  | 25           | 25           | 0.9                   |
| 0.05  | 0.26  | 35           | 45           | 8.4                   |
| 0.10  | 0.40  | 35           | 45           | 16.1                  |
| 0.20  | 0.53  | 35           | 45           | 28.2                  |
| 0.40  | 0.73  | 35           | 45           | 44.8                  |
| 0.80  | 1.13  | 35           | 45           | 88.9                  |

**Table 2.** Effect of the initial crack size on source parameters for initial damage  $D_0 = 0.1$ .  
See Figure 1 for definitions of the various radii.  
(from Johnson and Sammis, 2001)

| $a$<br>(cm) | $D_f$ | $r_f$<br>(m) | $r_d$<br>(m) | $V_{max}$<br>(cm/sec) |
|-------------|-------|--------------|--------------|-----------------------|
| 0.01        | 0.22  | 18           | 18           | 2.6                   |
| 0.10        | 0.40  | 35           | 45           | 16.1                  |
| 1.00        | 0.39  | 75           | 90           | 21.1                  |
| 10.0        | 0.40  | 90           | 150          | 13.1                  |

Note that increasing the initial damage at constant flaw size (Table 1) has little effect on either the failure radius or the damage radius but it does increase the maximum particle velocity in the source. Increasing the flaw size at constant damage (Table 2) produces a significant increase in

both the failure radius and the damage radius, but has less effect on the maximum velocity. Russian experiments have found that extensive fracturing extends to  $40 - 200 \text{ m/kt}^{1/3}$ . Since the yield of the NPE experiment was 1.07 kt, these numbers are consistent with the damage radii from Table 2 if the flaw size  $a$  is in the mm – cm range.

## RESEARCH ACCOMPLISHED

### Scaling of Secondary Radiation from Nuclear Explosions

Over the past three years, we have applied the approach in Johnson and Sammis (2001) to the US nuclear explosions in granite: HARDHAT, SHOAL, and PILEDRIIVER. The source parameters for these events, and the NPE chemical explosion, are given in Table 3.

**Table 3.** Source parameters for explosions in this study.

|             | <i>Yield<br/>(kt)</i> | <i>Depth<br/>(m)</i> | <i><math>W^{1/3}</math></i> | <i>Cavity Radius<br/>(m)</i> |
|-------------|-----------------------|----------------------|-----------------------------|------------------------------|
| NPE         | 1.07                  | 389                  | 1.02                        | 15                           |
| HARDHAT     | 5.7                   | 287                  | 1.79                        | 19.2                         |
| SHOAL       | 12                    | 367                  | 2.29                        | 26.8                         |
| PILEDRIIVER | 62                    | 463                  | 3.96                        | 40.1                         |

The cavity radii are plotted in Figure 5.

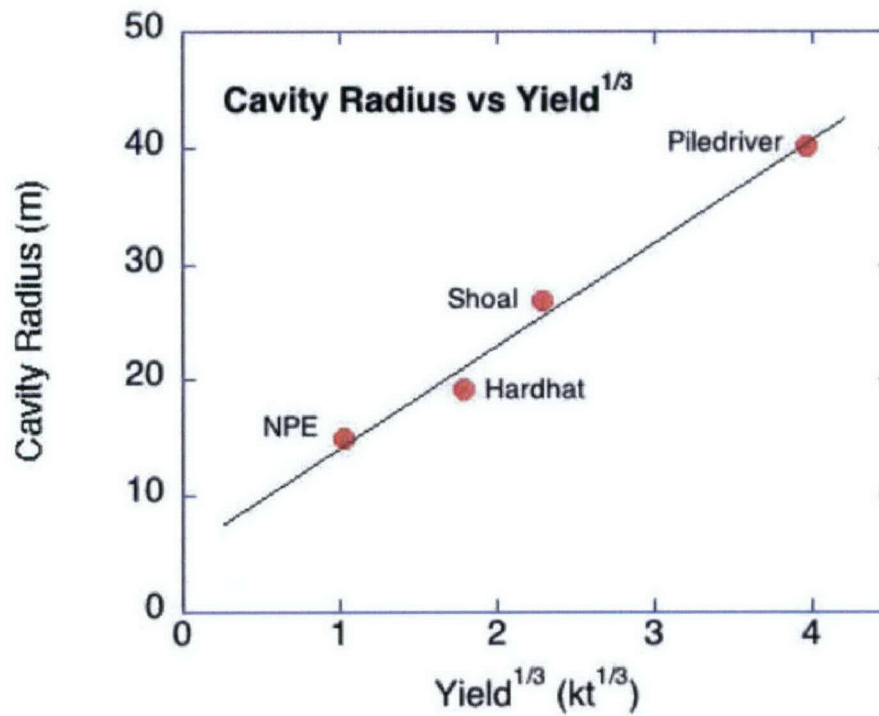


**Figure 5.** Cavity radius vs yield for modeled explosions.

The source parameters found by our model are given in Table 4 for the case of no prestress and in Table 5 for the case of 100MPa prestress.

**Table 4.** Source radii for case of no prestress.  $D_o = 0.1$ ,  $a = 1cm$   
See Figure 1 for definitions of the various radii.

|             | Cavity Radius<br>$r_c (m)$ | Failure Radius<br>$r_f (m)$ | Damage Radius<br>$r_d (m)$ | Slip Radius<br>$r_e (m)$ |
|-------------|----------------------------|-----------------------------|----------------------------|--------------------------|
| NPE         | 15                         | 75                          | 90                         |                          |
| HARDHAT     | 19.2                       | 150                         | 250                        | >1000                    |
| SHOAL       | 26.8                       | 250                         | 250                        | >1000                    |
| PILEDRIIVER | 40.1                       | 450                         | 550                        | >1000                    |

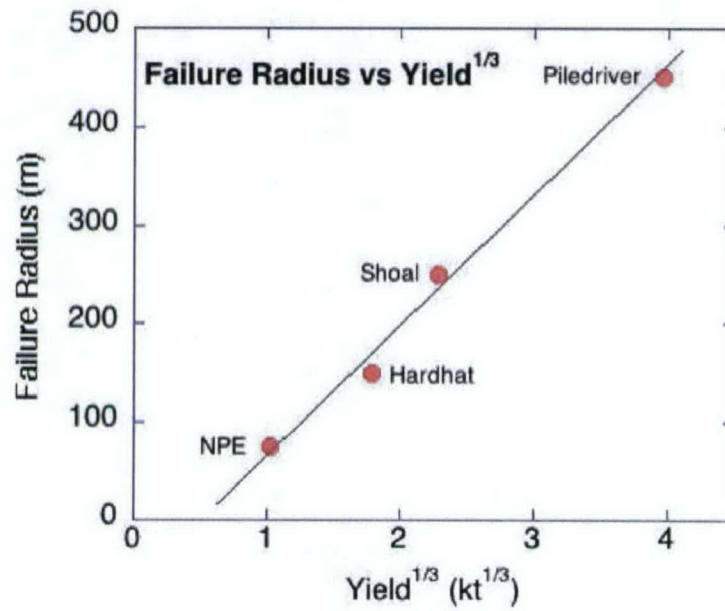
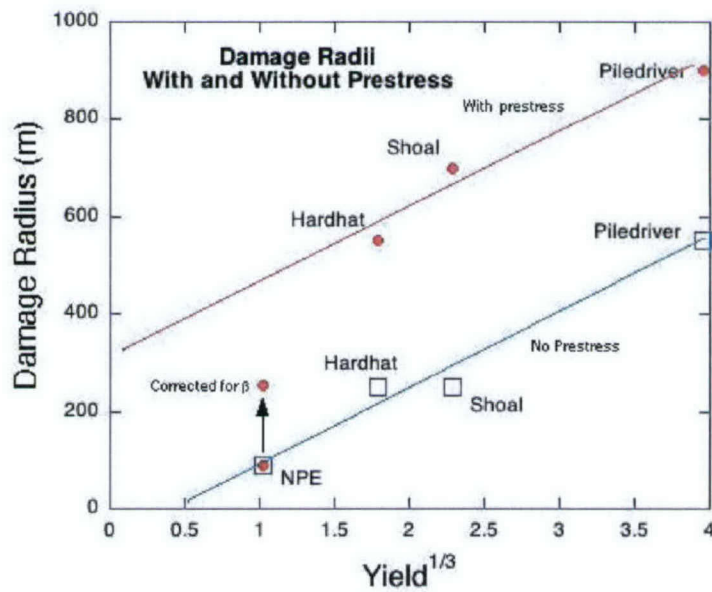


Figure 6. Failure radius vs yield<sup>1/3</sup> for the case of no prestress.  $D_o = 0.1$ ,  $a = 1cm$ .

**Table 4.** Source radii for case of prestress.  $D_o = 0.1$ ,  $a = 1cm$   
See Figure 1 for definitions of the various radii.

|             | Cavity Radius<br>$r_c(m)$ | Failure Radius<br>$r_f(m)$ | Damage Radius<br>$r_d(m)$ | Elastic Rad.<br>$r_e(m)$ |
|-------------|---------------------------|----------------------------|---------------------------|--------------------------|
| NPE         | 15                        | 75                         | 90                        | 116                      |
| HARDHAT     | 19.2                      | 550 ±100                   | 550 ±100                  | 704                      |
| SHOAL       | 26.8                      | 550 ±100                   | 700 ±100                  | 915                      |
| PILEDRIIVER | 40.1                      | 900 ±100                   | 900 ±100                  | 1280                     |



**Figure 7.** Comparison of damage radius vs yield<sup>1/3</sup> for the cases of prestress and no prestress.  $D_o = 0.1$ ,  $a = 1cm$ . Note that the value of NPE has been corrected for the lower shear wave velocity in tuff as compared with granite for the other explosions. The prestress significantly increases the damage radius at a given yield.

The secondary seismic radiation calculated for the four explosions is shown in Figures 8-11.

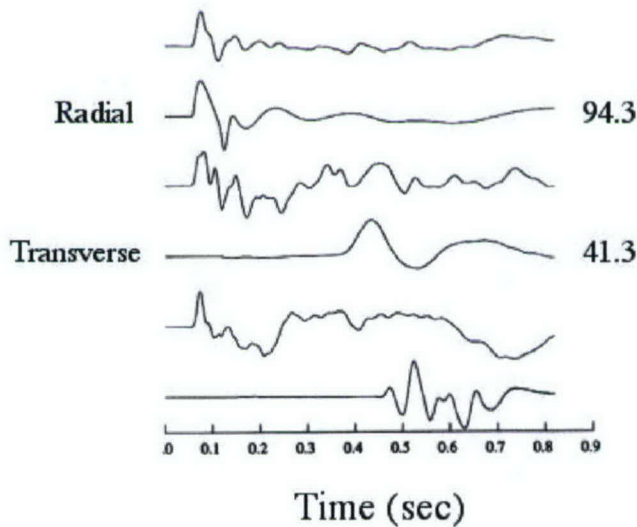


**Figure 8.** Secondary seismic radiation calculated for the NPE chemical explosion

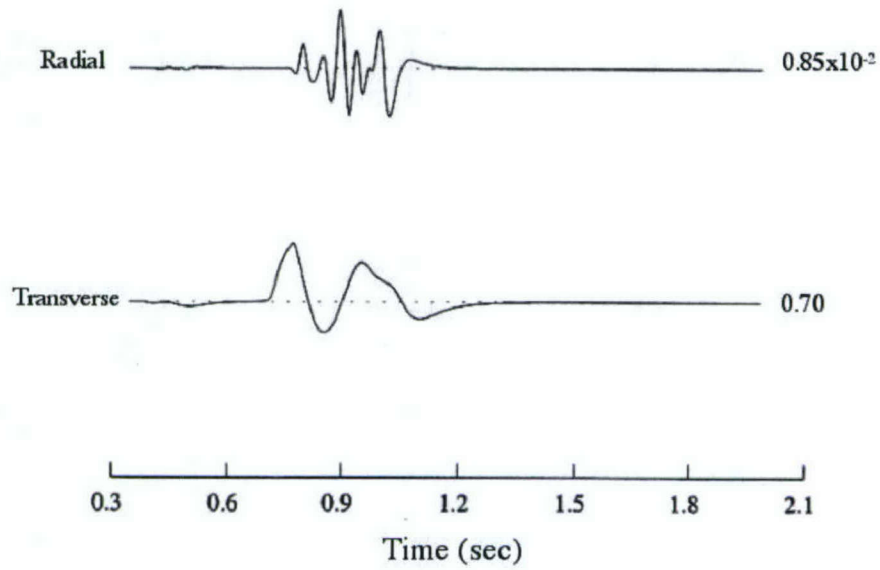


**Figure 9.** Secondary seismic radiation calculated for the HARDHAT nuclear explosion.

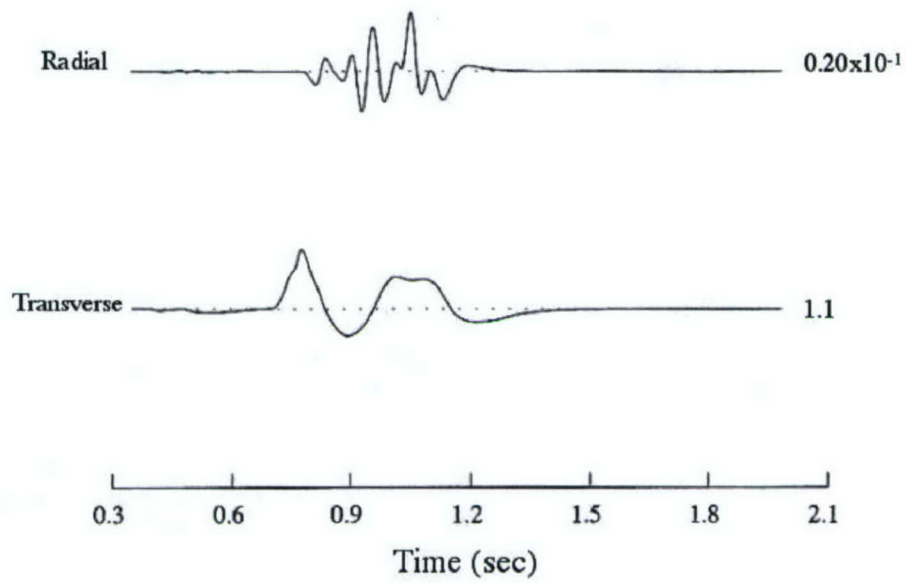


**Figure 10.** Secondary seismic radiation calculated for the SHOAL nuclear explosion.

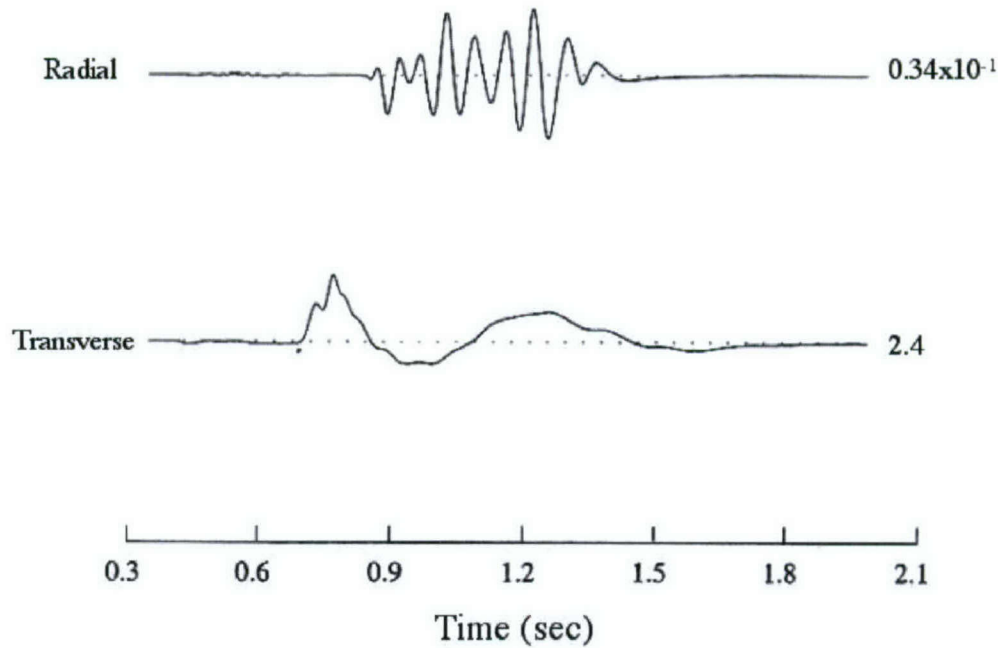


**Figure 11.** Secondary seismic radiation calculated for the PILED DRIVER nuclear explosion.

The transverse components are compared in Figure 12.

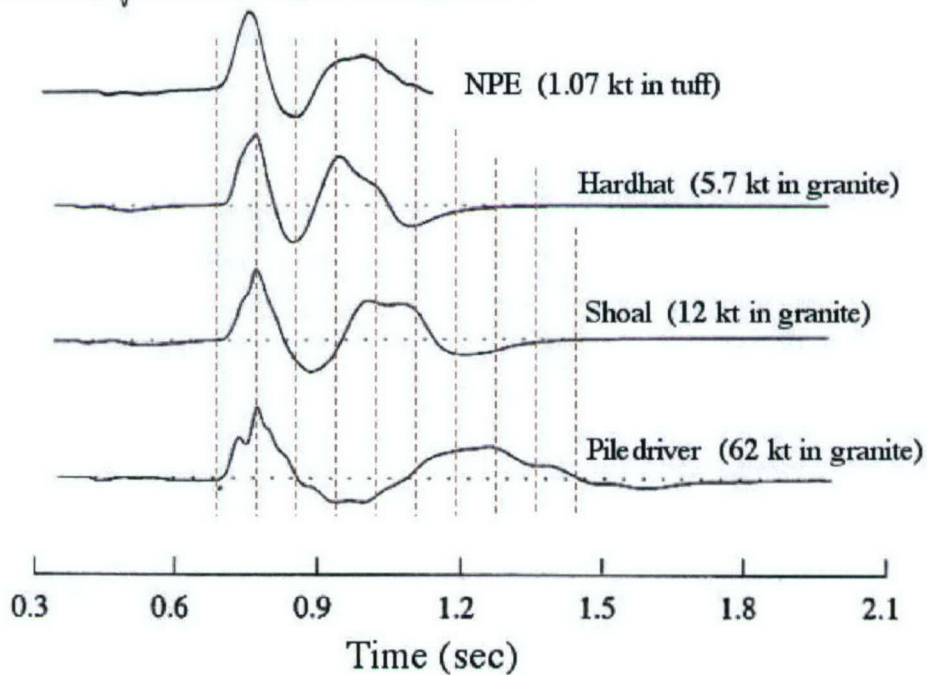


**Figure 12.** Comparison of the transverse components of the secondary radiation generated by the four explosions.

In Figure 13, the time axes are rescaled and the frequency of the first half-cycle is measured.

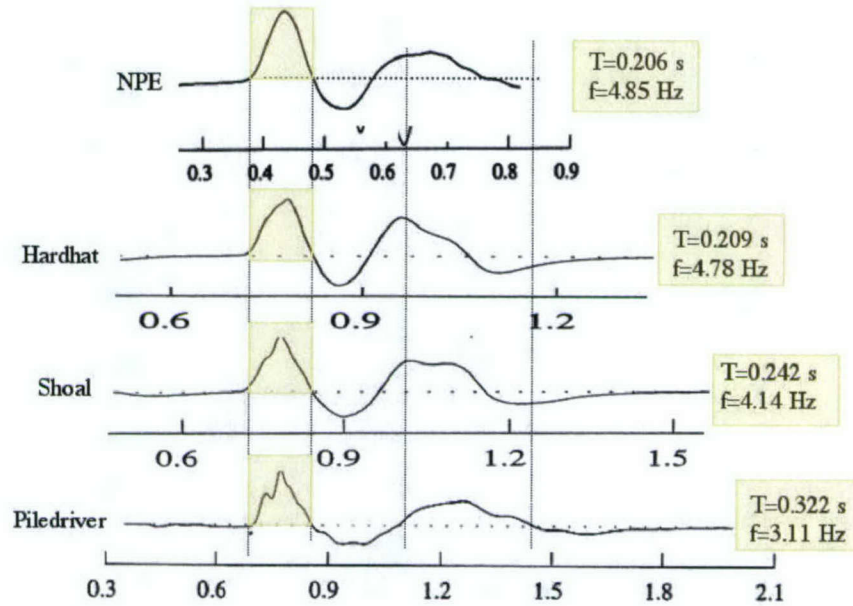


**Figure13.** Rescaling of the transverse components of the secondary radiation from Fig. 12.

The seismic radius is calculated from the period as indicated in Table 5 where it is compared to the damage radius. This comparison is also made in Figure 14.

**Table 5.** Seismic radius, calculated from the period of the first cycle of the secondary radiation, is compared with the damage radius found above.

|             | $r = \beta T$ (m) | Damage $r(m)$ |
|-------------|-------------------|---------------|
| NPE         | 247               | 90            |
| HARDHAT     | 706               | 550           |
| SHOAL       | 818               | 700           |
| PILEDRIIVER | 1088              | 900           |

The shear wave velocity for granite is  $\beta = 3.38$  km/s and for tuff  $\beta = 1.2$  km/s.

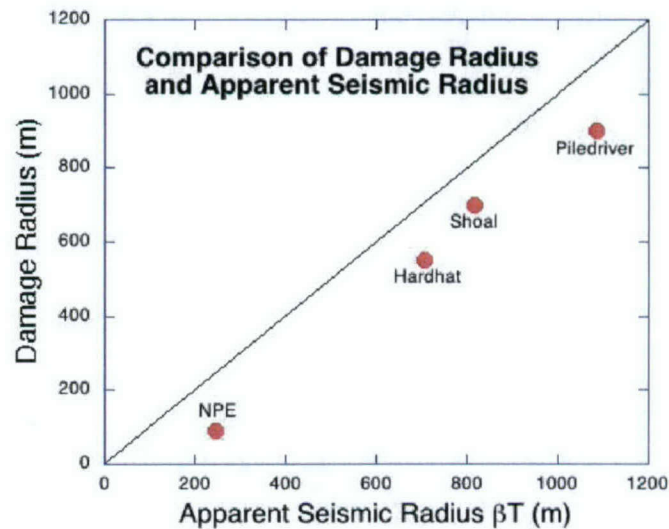


**Figure 14.** Comparison of the damage radius found from the model and the apparent seismic radius calculated from the spectral content of the theoretical secondary S wave radiation.

*The effect of frozen rock on seismic coupling*

At the very end of this contract period, we did a preliminary analysis of data from Mellor (1973) who measured the uniaxial compressive and tensile strengths of granite, limestone, and sandstone over a range of temperatures from 20°C to -197°C. His data are replotted in Figures 15 and 16. For each of the three rock types, he tested both air-dry and water-saturated samples.

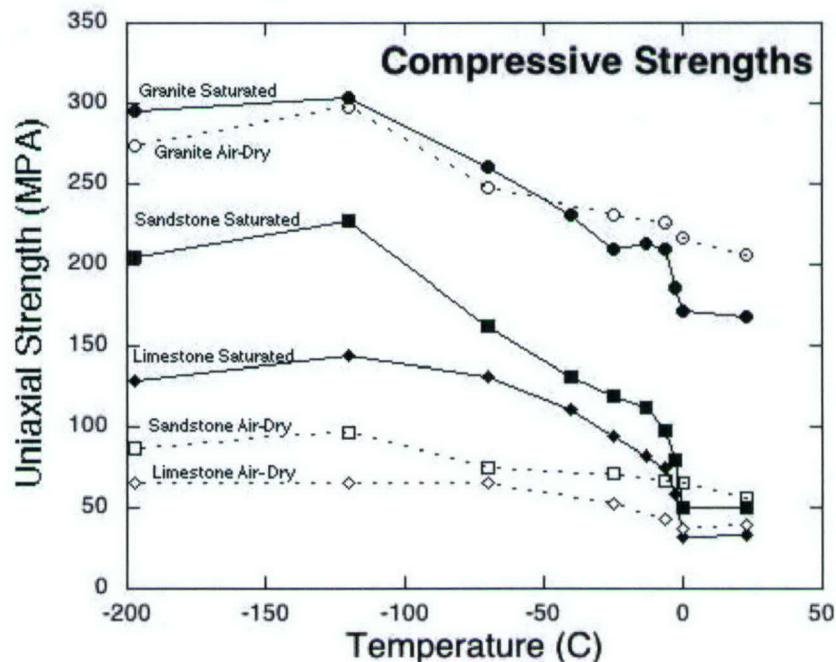


**Figure 15.** Uniaxial compressive strengths of saturated and air-dry rock as a function of temperature from 20° C to -196° C.

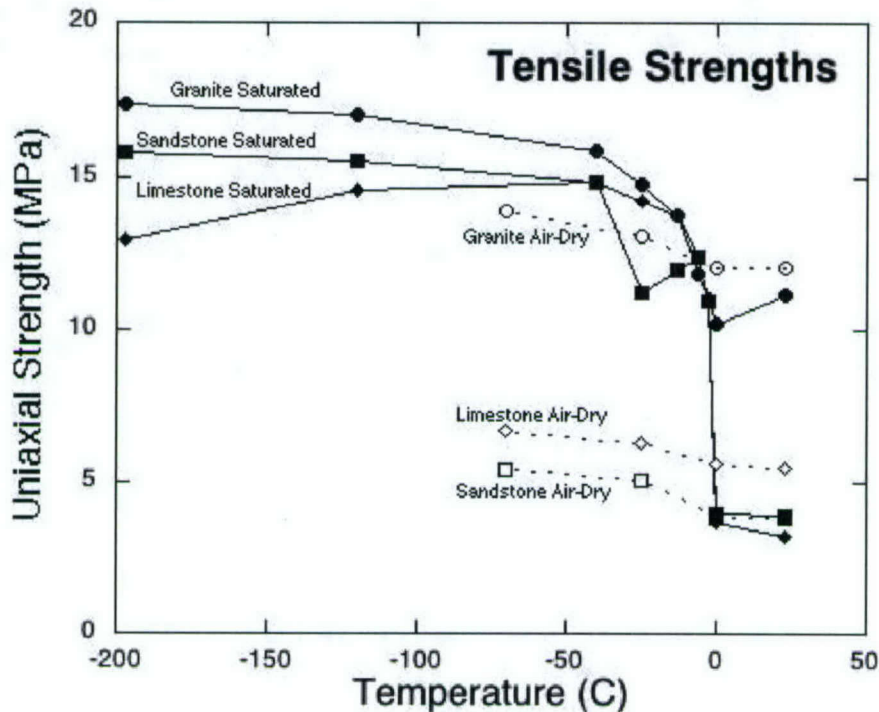


**Figure 16.** Uniaxial tensile strengths of saturated and air-dry rock as a function of temperature from 20° C to -196° C.

There are a some interesting observations regarding these data that can be explained by assuming that the behavior is controlled by frozen water in the cracks:

Observation 1: Increase in strength beginning at 0° C and continuing to -120° C. No further increase between -120° C and -197° C

Explanation 1: Frozen water inhibits sliding on the preexisting flaws, suppressing further damage thereby strengthening the samples. The crack-bridging ice asperities creep most at 0° C, and progressively less at lower temperatures. Below 120° C, ice deforms by temperature-independent dislocation glide.

Observation 2: Air-dry granite shows the same strengthening at low temperatures as does saturated granite.

Explanation 2: The microcracks that comprise the initial damage in granite are so thin that they are effectively saturated by water films in the air-dry samples.

Observation 3: The tensile strength of all saturated samples is greater than that of the air-dry samples.

Explanation 3: Tensile failure nucleates at the largest flaw in each sample. Even in granite, this largest flaw is not saturated by the water films in the air-dry state.

We modeled these data using the micromechanical damage model formulated by Ashby and Sammis (1990) by assuming that the primary role of the frozen water in the cracks is to increase

the coefficient of friction through the formation of crack-bridging "ice asperities" in addition to the usual rock asperities. Figure 17 shows the coefficient of friction in the sliding cracks required to produce the increase in compressive strength of granite in Figure 15.

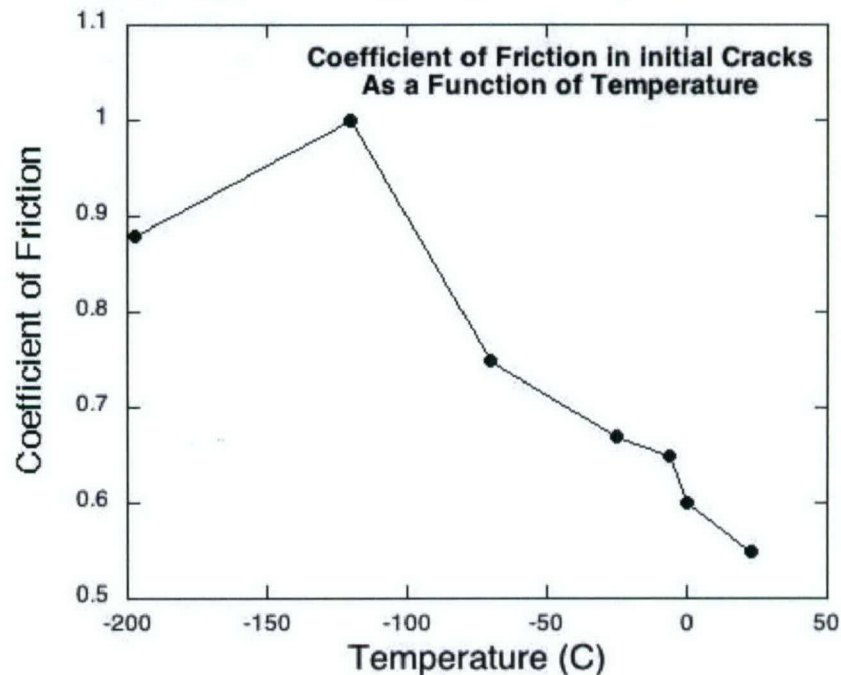


**Figure 17.** The coefficient of friction required at each temperature if the damage mechanics model is to fit the compressive failure data for granite in Figure 15.

The rock asperities are far below their melting temperature and deform by dislocation glide, which is only weakly temperature dependent. The ice asperities, however, form at their melting temperature and therefore deform initially by diffusion-limited creep mechanisms, which are strongly temperature dependent. The strengthening of the ice asperities with falling temperature explains the observed monotonic increase in compressive and tensile strengths at progressively lower temperatures. It also explains the leveling off of strength at very low temperatures where ice is sufficiently below its melting temperature that it deforms by glide, just like the rock asperities. The model is most suitable for low porosity crystalline rock like granite where Mellor (1973) observed a 35% increase in compressive and a 55% increase in tensile strength between 0 and -120°C.

One important implication of our model is that the effective coefficient of friction, and hence the compressive strength, is both temperature and strain-rate dependent. At the high strain rates in an explosive source, the 35% increase in strength should occur over a much smaller range of temperatures close to 0°C. The observed strengthening in granite is the same for both the air-dry and saturated samples whereas in both limestone and sandstone the saturated samples strengthen much more than do the air-dry samples. This is probably due to the fact that the starter flaws in granite are very thin cracks which are effectively saturated by adhered water films in the air-dry state, while the filling of the more spherical pores in the sandstone and, to a lesser extent, the limestone preferentially increases their mechanical strength in the saturated frozen state. The damage mechanics model is able to qualitatively and quantitatively explain all observed

differences between the low temperature behavior of the three rock types and between the dry and saturated states in each. This preliminary assessment of the mechanisms responsible for strengthening rock at low temperature should help guide the design of future low-temperature experiments, and suggests that low-temperature triaxial strength testing should be supplemented with low-temperature friction experiments.

## SUMMARY AND CONCLUSIONS

To summarize, the model-based damage mechanics developed by Ashby and Sammis (1990) has been used in conjunction with the effective medium model (Johnson, 1996) to study the scaling properties of fracture damage generated by underground explosions. Prior work by Johnson and Sammis (2001) has been extended by modeling three U.S. nuclear explosions in granite: HARDHAT, SHOAL, and PILEDRIIVER. Both the failure radius and damage radius were shown to scale as yield to the one-third power. More importantly, this model predicts that the secondary seismic radiation generated by the damage process makes a significant contribution to the P wave radiation and that any preferred orientation of the preexisting fracture sets in crystalline rock leads to the generation of significant S wave energy which could effect source detection and discrimination algorithms. The period of this secondary radiation was also found to scale as yield<sup>1/3</sup>.

We also began a preliminary investigation into the strength of frozen rock. The progressive strengthening of granite with falling temperature below zero was shown to be consistent with the assumption that it is due to frozen water in the fractures. The Ashby and Sammis (1990) damage mechanics gives a quantitative description of this strengthening. Since this damage mechanics is already incorporated in the Johnson (1996) source model as well as Jeff Stevens more sophisticated numerical models, it should be relatively simple to test the effect of frozen rock on seismic coupling.

## REFERENCES

- Ashby, M.F., and C.G. Sammis, The damage mechanics of brittle solids in compression, PAGEOPH, 133, 489-521, 1990.
- Denny, M. D., Introduction and highlights. In Proc. Symposium on the Non-Proliferation Experiment (NPE): Results and Implications for Test Ban Treaties (ed. M. D. Denny), CONF-9404100 (Department of Energy, 1994).
- Glenn, L. A., Energy-density Effects on Seismic Decoupling, J. Geophys. Res. 98, 1933-1942, 1993.
- Glenn, L. A., and Goldstein, Seismic Decoupling with Chemical and Nuclear Explosions in Salt, J. Geophys. Res. 99, 11,723-11,730, 1994.
- Johnson, L.R., The effect of damage on explosion generated elastic waves, Proceedings of the 18th annual seismic research symposium on monitoring a comprehensive test ban treaty, 4-6 September 1996, 195-198, 1996.
- Johnson, L.R., and C.G. Sammis, Effects of rock damage on seismic waves generated by explosions, PAGEOPH, 158, 1869-1908, 2001.

- King, D. S., Freeman, B. E., Eilers, D. D., and Johnson, J. D., The Effective Yield of a Nuclear Explosion in a Small Cavity in Geologic Material: Enhanced Coupling Revisited, *J. Geophys. Res.* 94, 12,375-12,385, 1989.
- Mellor, M. (1973), Mechanical properties of rocks at low temperatures, Second International Conference on Permafrost, National Academy of Sciences, Washington, D.C., 334-343, 1973.
- O'Connell, R. J., and Budianski, B. Seismic Velocities in Dry and Saturated Cracked Solids, *J. Geophys. Res.* 79, 5412-5426. 1974.
- Rimer, N., J.L. Stevens, and S.M. Day, Effect of pore pressure, fractures, and dilatancy on ground motion in granite, S-Cubed Report SSS-R-87-8670, 1987.
- Rimer, N., Stevens, J. L., Murphy, J. R., and Kocharyan, G. G. Estimating seismic characteristics of explosions in hard rock using a micro-mechanical damage model. In *Proc. 20th Annual Seismic Research Symposium on Monitoring a Comprehensive Test Ban Treaty* (eds. J. Fantroy, D. Heatley, J. Warren, F. Chavez, and C. Meade) (Department of Defense and U.S. Department of Energy), pp. 392-400, 1998.
- Rimer, N., J. L. Stevens, J. R. Murphy, and G. G. Kocharyan, Estimating Seismic Source Characteristics of Explosions in Hardrock Using a Micromechanical Damage Model, Maxwell Technologies Final Report MTSD-DFR-99-16423, 1999..
- Rodean, H. C., Nuclear-Explosion Seismology, TID-25572, (U. S. Atomic Energy Commission, 156 pp., 1971.
- Stevens, J. L., N. Rimer, H. Xu, J. R. Murphy, G. E. Baker, G. G. Kocharyan, B. A. Ivanov, and S. M. Day, Near Field and Regional Modeling of Explosions at the Degelen Test Site, *Proceedings of the 24<sup>th</sup> Seismic Research Review – Nuclear Explosion Monitoring: Innovation and Integration*, Sept. 17-19, 2002, Ponte Verde Beach, Florida, 562-571, 2002.